PERGAMON

Computerized Medical Imaging and Graphics 24 (2000) 389–406

Computerized Medical Imaging and Graphics

www.elsevier.com/locate/compmedimag

Advances in three-dimensional reconstruction of the experimental spinal cord injury

B.S. Duerstock[a], C.L. Bajaj[b], V. Pascucci[c], D. Schikore[d], K.N. Lin[e], R.B. Borgens[a,*]

[a]*Department of Basic Medical Sciences, School of Veterinary Medicine, Center for Paralysis Research, Purdue University, 1244 VCPR West Lafayette, IN 47907-1244, USA*

[b]*Department of Computer Sciences, Center for Computational Visualization, The University of Texas at Austin, Austin, TX, USA*

[c]*Lawrence Livermore National Laboratory Livermore, CA, USA*

[d]*Computational Engineering International, Morrisville, NC, USA*

[e]*Foundry Networks, Inc. San Jose, CA, USA*

Received 1 November 1999; accepted 6 June 2000

Abstract

Three-dimensional (3D) computer reconstruction is an ideal tool for evaluating the centralized pathology of mammalian spinal cord injury (SCI) where multiple anatomical features are embedded within each other. Here, we evaluate three different reconstruction algorithms to three-dimensionally visualize SCIs. We also show for the first time, that determination of the volume and surface area of pathological features is possible using the reconstructed 3D images themselves. We compare these measurements to those calculated by older morphometric approaches. Finally, we demonstrate dynamic navigation into a 3D spinal cord reconstruction.

Keywords: Three-dimensional reconstruction; 3D Computer visualization; 3D Morphometry; Spinal cord injury; Neurotrauma; Serial light microscopy; Registration

1. Introduction

For over 30 years the ability to construct three-dimensional (3D) images from biological specimens using the computer has been expanding with technological advances in both hardware and software [1]. In recent times, certain areas of biological and medical imaging have been particularly innovative in producing 3D images of acquired two-dimensional (2D) data sets because the acquisition techniques are conducive to 3D reconstruction. Examples would include the reconstruction of Magnetic Resonance Images and Computer Tomography in Medicine, and 3D visualization of Confocal Laser and Scanning Electron Micrographs in biology [2,3]. These acquisition technologies provide ease in reconstruction since the registration of serial images is automated.

Though such techniques are powerful, they are not as universally utilized in experimental biology and medicine as is light microscopy (LM). The compound light microscope still provides investigators high levels of resolution in concert with many types of specific cell identification. The modern light microscope provides the broadest range of examination, from the subcellular to the tissue level of investigation on one platform. Where once conventional photography was married to light microscopy, the darkroom has been replaced by image digitization using video cameras mounted to the microscope. In spite of these developments, it is not a common feature of modern LM systems to possess 3D reconstruction programs as the issues of registration of serial sections, contour tracing techniques, section distortion, and the completeness and suitability of the data set for 3D imaging are still daunting problems.

One particular area of need is laboratory-based research in spinal cord injury. These injuries are both intractable and present a growing dilemma to both healthcare and society at large [4]. Experimental treatments to rodent models have traditionally been the means of developing medical interventions such as the acute administration of methylprednisolone [5]. Manipulation of such experimental injuries not only requires careful selection of behavioral models [6], but the means to detect subtle pathological changes in the

* Corresponding author. Tel.: +1-765-494-7600; fax: +1-765-494-7605.
E-mail address: cpr@vet.purdue.edu (R.B. Borgens).

0895-6111/00/$ - see front matter
PII: S0895-6111(00)00034-3

anatomy of the injury. This is an ideal area of study to apply 3D based techniques to the morphometry of complicated histological material.

Here we describe and compare three types of 3D visualization techniques. We evaluated 3D images derived from: (1) volumetric texture imaging algorithms; (2) surface tiling algorithms; and (3) isocontouring algorithms. We compare and contrast approaches for 2D image registration, contour and object selection, image enhancement and filtering, 3D image transparency, and the dynamic navigation of the "observer" into these 3D reconstructions.

The capability to quantify the 3D reconstruction may be equally if not more valuable than revealing the shapes of 3D structures. Past quantitative methods used either a 2D morphometric approach [2,3,7–11] to derive volumes and surface areas from the data sets that make up the 3D reconstruction or through the use of mathematical formulas for geometric shapes that may have a similar morphology to the area of interest [7,8,12,13]. We believe this examination of techniques is the first to both evaluate and contrast different mathematical approaches for the 3D reconstruction of soft tissue injury, in particular the spinal cord, and to calculate the volume and surface area of various structures from the actual 3D images themselves.

2. Materials and methods

2.1. General procedures

Fully adult (300 g) laboratory rats (Sprague-Dawley) were used in these experiments. Following experimental injury to the spinal cord (see below), they were housed two animals per cage, fed ad libidum, and their health monitored daily. Three animals in this study were sacrificed 19, 20, and 180 days post-surgery by an overdose of Sodium Pentobarbital (0.8 ml of 1 g/ml standard injectable) immediately followed by perfusion/fixation with 6% paraformaldehyde, 0.1% glutaraldehyde in a phosphate buffer. The spinal cords were dissected free and immersion fixed in the above fixative for about 18 h. One animal that was not injured was sacrificed and the spinal cord was then perfused and fixed in the same manner.

2.2. Experimental spinal cord injury

Anesthesia was performed using an intraperitoneal injection of 0.1 ml/100 g body weight of a standardized solution of 10 ml Ketamine HCL (100 mg/ml) and 1.1 ml Xylazine (20 mg/ml). The spinal cord was exposed by a partial laminectomy (10th to 11th thoracic vertebrae; dura left intact) and the dorsal hemisphere crushed using blunted Watchmakers forceps in two cases. In a third animal, a piercing injury to the cord was made with sharpened forceps and a ca. 0.5 mm piece of striated muscle was inserted as an autogenic tissue graft to the cord. All incisions were closed in layers with 3–0 proline suture, and the skin closed with wound clips. Immediately post-surgery each animal was subcutaneously injected with 3 ml lactated ringers to prevent dehydration, and the animal placed under a heat lamp for about 24 h to reduce post-surgical mortality due to shock.

2.3. Immunocytochemistry and staining

The segments of spinal cord (ca. 1 cm in length) containing the area of experimental injury were dehydrated in ascending concentrations of alcohol followed by xylene permitting infiltration and embedding in Paraplast (paraffin) by conventional methods. The entire segment was sectioned on a rotary microtome at approximately 15 μm, and these horizontal longitudinal sections were affixed to microscope slides. Prior to use the slides were dipped in a 0.5% gelatin solution which aids in the adhesion of the sections to the slides during subsequent treatment. Paraffin was partially removed with a 1 h treatment in a 60°C oven, and completely removed after a 1 h immersion in 100% xylene. Sections were rehydrated by immersions in descending grades of alcohol to distilled water by conventional methods. Hydrated sections from the crush injuries were incubated in a commercial enzyme and tissue nonspecific antigen blocker (Endo/Blocker M69 and Tissue Blocker, Biomeda) for 5 min, with a 1 min rinse in buffer (Automation Buffer, Biomeda). The sections were then exposed to the primary antibody for the macrophage, ED1 [MCA-341, Serotech/Harlan Bioproducts (mouse antirat)] for 10 min, and rinsed with buffer. This dominant cell type has been useful in establishing the boundaries of the lesion at the acute and subacute phase of injury [14,15]. The secondary biotinylated antibody [rabbit-antimouse (Lab/Probe, Biomeda)] was administered for 10 min, rinsed in buffer prior to exposure to the streptavidin peroxidase (10 min), rinsed, and exposed to a commercially prepared Diaminobenzidine reagent (Biomeda) for 5 min, and counter-stained with hematoxylin. Stained sections were rinsed in distilled water and coverslip affixed with a warm glycerol gelatin (Sigma Chemical Co.). The transplant specimen was sacrificed at 180 days post-injury, embedded and sectioned as previously described, but the sections were only stained with hematoxylin. The uninjured spinal cord segment was immersed in a 10% sucrose solution in a phosphate buffer before being quick frozen in liquid nitrogen, sectioned on a freezing microtome (40 μm), mounted on microscope slides, and stained with hematoxylin and eosin.

2.4. Video frame grabbing and image reproduction

Viewing of spinal cord sections was accomplished with an Olympus Van Ox Universal Microscope. A JVC TK-1070U color video camera mounted on the microscope displayed histological sections on a computer monitor. Images were acquired to a Macintosh Quadra 800 computer with RasterOps®, MediaGrabber™ software, and managed on a dual Pentium Pro computer using Adobe Photoshop®

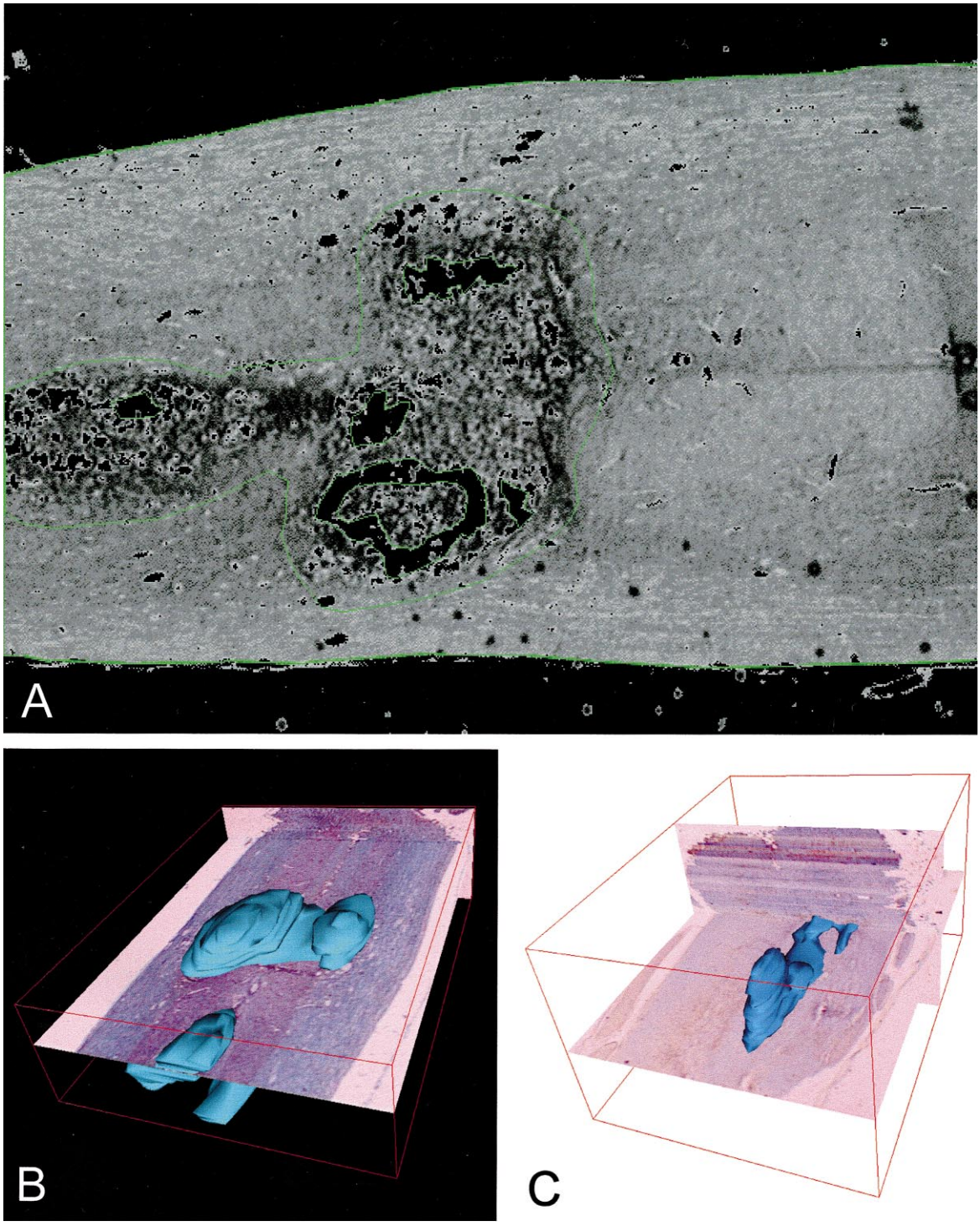

Fig. 1. Three-dimensional reconstruction of defined regions of interest by surface tiling algorithms. In (A), the photomicrograph of one longitudinal/horizontal section of an injured spinal cord reveals several external and internal features for 3D reconstruction. The perimeters of the tissue section, the central region of injury, and the largest cystic cavities within this region of injury have been circumscribed in green. The injury zone was defined by ED1 monoclonal antibody (refer to Methods). The large cysts were apparent against the background staining of this tissue. This histological section is approximately 15 μm in thickness and 2.6 mm at its widest point. The left margin of the spinal cord is rostral and the right, caudal. A similar set of boundaries was produced for every histological section comprising the entire spinal segment for subsequent reconstruction. The histological slice in (A) was one from the data set used to construct the 3D image shown in (B). In (B), the 3D reconstruction of the injured spinal tissue is shown in blue. This was embedded within one of the longitudinal/horizontal sections used to produce the overall 3D image (~80 fifteen μm sections). This plane of section can be dynamically shifted through the 3D image to demonstrate the registration of the injury within the spinal cord data set. This segment of spinal cord containing the lesion was about half of the vertebral segment. Following reconstruction, a transverse plane may be generated though this spinal cord segment as shown in the upper right plane — though this was not the plane of original sectioning. This was even more apparent in the surface reconstruction shown in (C). This was another injured spinal segment, three weeks post-injury, where the injury site is shown in blue (~130 longitudinal/horizontal sections at 15 μm thickness). In both (B) and (C) the ventral surface of the spinal cord is facing upwards, in B the rostral end forward and C the caudal end forward.

software. Color plates were produced using Microsoft PowerPoint® software and prints were produced on an Epson Stylus Color 800 printer and a Tektronix Phaser 440 dye-sublimation color printer.

2.5. Registration of serial sections for three-dimensional visualization

For 3D surface reconstruction and volume visualization, the spinal cord segment containing the lesion was acquired to the computer at low magnification (20×). Every serial histological section comprising a spinal cord segment was used for reconstruction. Registration was accomplished by superimposing each successive digitized histological section one after another by the investigator. This was accomplished by positioning and rotating the microscope stage to achieve the "best-fit" of superimposed consecutive images. The boundary of the spinal cord and many other anatomical characteristics provide numerous fiducial points or objects (such as cysts, central canal, and general features of the lesion) to serve in optimal serial registration (see also Ref. [14]).

2.6. Conversion of data set files

Each of the three visualization methods applied in this study involved converting the series of captured histological slices in order to obtain the correct file type. These visualization algorithms required the use of greyscale images with a reduced range of pixel values from 0 to 255.

2.7. Computer science approach to software development

2.7.1. Algorithm: volumetric texture imaging

Volume rendering [16] is a useful technique for visualizing 3D volumetric data sets like CT or MRI scans. In these cases the volumetric data set is obtained by stacking a sequence of 2D pictures one on top of the other forming a 3D regular grid of RGB (Red Green Blue) values: one RGB value per voxel. Volume rendering provides a way to see through the entire 3D data by modeling the level of transparency associated to the RGB values.

Ray casting techniques [17] render the volume by shooting one ray per display pixel. However, advances in graphics hardware for texture mapping allowed the development of a more efficient volume rendering approach [18]. The 3D volumetric data set is stored in the 3D Texture Mapping memory of a high-end graphics workstation. In this way, the 3D volume can be sliced by using the capability of the graphics hardware to compute slices of the 3D texture map.

Three kinds of explorations of the volume were allowed by this approach. First, there was a basic change of view exploration. Second, clipping the volume into multiple planes in any arbitrary position allowed views into internal regions that were otherwise hidden. Third, different ranges of colors and levels of transparency could be applied to the 3D volume.

2.7.2. Algorithm: surface tiling reconstruction

We employed a novel 3D reconstruction algorithm proposed in Bajaj et al. [19], called Surface Tiling. This approach takes as input a data set of 2D polygonal slices in a sequence of parallel planes to produce a 3D surface [19,20]. Human intervention was required to define these planar polygons, called contours, around biological regions of interest from the sequence of histological images.

The novel surface tiling reconstruction method that we report here can be summarized in five main steps:

1. Form closed contours around areas of interest from the data set of digitized image slices. This is done by manual tracing.
2. The surface tiling algorithm determines the correspondence between the contours on the adjacent slices.
3. In a process called tiling, triangles are generated to form 3D surfaces connecting contours on the adjacent slices. The tiling rules were derived from surface criteria described in Bajaj et al. [19].
4. Some shapes which contain branching, dissimilar, or disappearing contours cannot be tiled based on the tiling rules. Therefore, new vertices must be added in the middle of two consecutive slices, so that the reconstructed tiled surface would satisfy the surface criteria [19].
5. Quantitative interrogation of Surface Tiled reconstructions is possible. The surface area is the total area of all tiled triangles. The volume of the region formed between two adjacent contours, defined as a prismatoid, can be calculated and summed for the entire 3D tiled surface [14,21].

2.7.2.1. Contour tracing for the surface tiling method. For surface tiling we use a computer program to trace contours on histological images with a mouse on a Sun SPARCstation IPX (Fig. 1). We employed a novel tracing program for contour selection that allows the user to see two previous tracings in the same window for comparison. Contours of interest were traced on each histological section of the spinal cord data set. Examples of such contours of interest circumscribed in each section included; the perimeter of the spinal cord segment, the injury site as defined, large cysts, and accumulations of macrophages.

2.7.3. Algorithm: isocontouring method

We used a third novel 3D reconstruction approach to produce isosurfaces, a complementary technique to volume rendering. From the same 3D volumetric data set that we used for volumetric texture imaging, one can extract surfaces of constant scalar values. To produce the

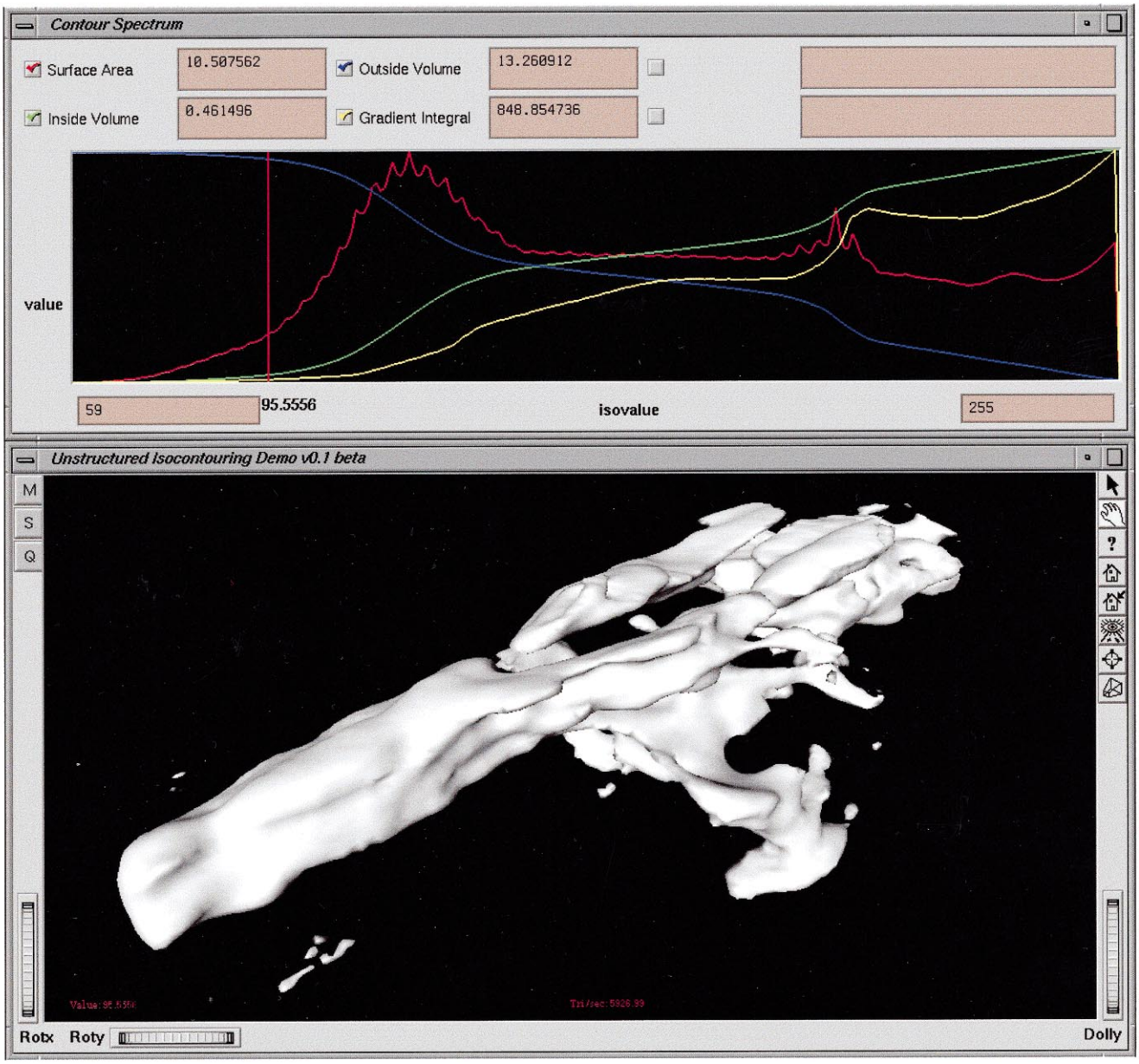

Fig. 2. Defining isocontours with pixel values and a graphical interface. This view shows two windows in which the isocontoured image is evaluated and above it, the isosurface pixel values used to produce it. The range of isovalues (59–255) is displayed for the investigator. The vertical (red) index line (set at 95.5556) can be moved along this gradient to arbitrarily increase or decrease the range of values used to produce the image displayed in the lower window. In this procedure the observer can subjectively define both the overall character of the image through topological changes. The surface area and volume measurements of the image are simultaneously changed as the index line is moved. This allows a real time evaluation of these quantitative factors while the three-dimensional image is managed. The image shown in this example is of a three-week old spinal cord injury defined by the staining of phagocytic cells that occupy this region in extreme numbers. This image was embedded within a segment of injured spinal cord and as well contained other pathological features such as large cysts and smaller cavitations. These features are displayed at other chosen isovalues. For example, an isovalue of approximately 146 displayed the cysts (Fig. 7F) but were not shown in this view. The image was altered in 3D space by the observer in the lower window, where the angle of view, amount of rotation, and panning of the image surface was accomplished.

isocontoured surfaces here, we have used the contour spectrum interface (Fig. 2) combined with the isosurface extraction algorithm proposed in Bajaj et al. [22]. “Contour Spectrum” efficiently precomputes a set of index signatures of a given scalar field. Each signature is a function of the field value space such as the size of the surface area (red) and the volume (green and blue) contained in each isosurface for any specified isovalue. The plot of the signatures provides an interface that aids the user in selecting the desired isosurface (Fig. 2, top). We used this spectrum analysis to select anatomical structures of the spinal cord segments to be three-dimensionally reconstructed. Isovalues were chosen at distinct features of the waveforms that indicated the presence of prominent isosurfaces in the data set

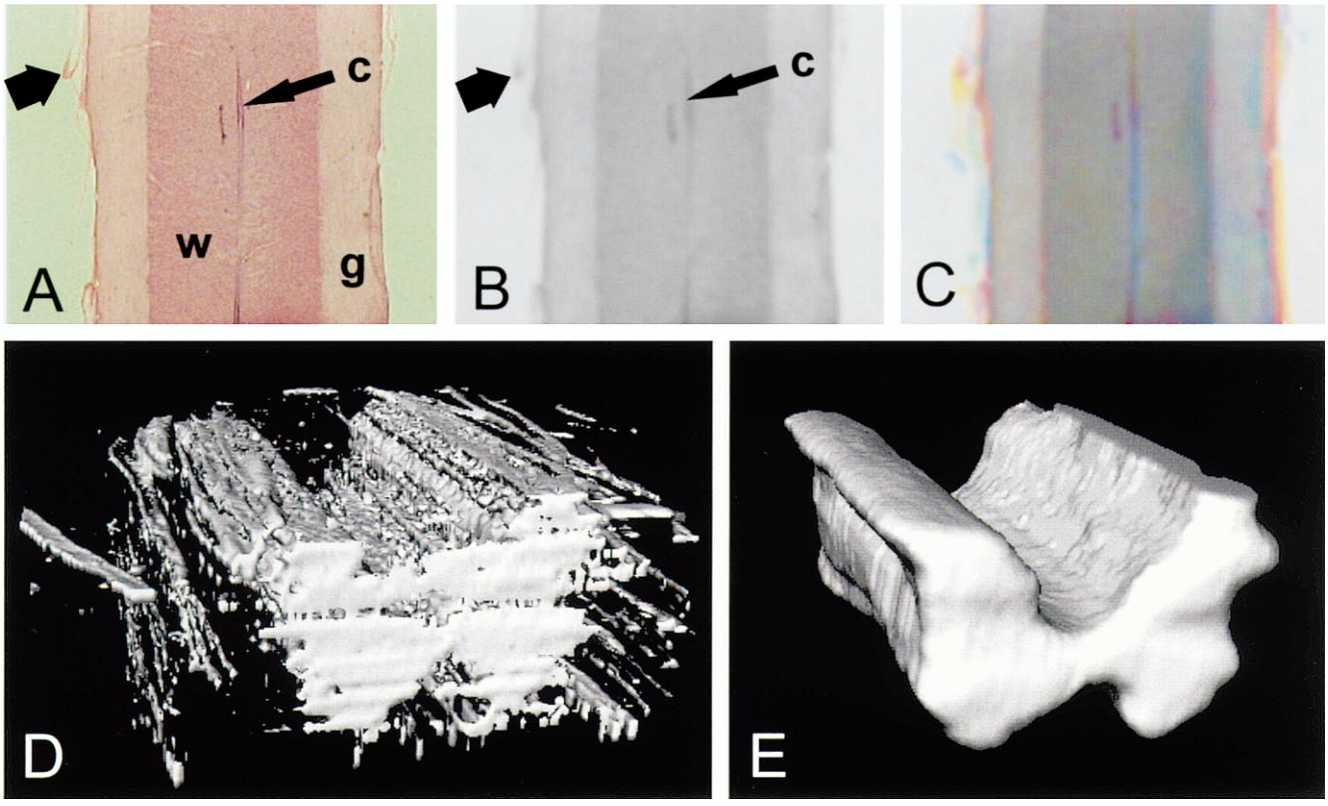

Fig. 3. Filtering the image prior to three-dimensional reconstruction with isocontouring algorithms. In (A), (B), and (C), identical longitudinal/horizontal histological sections of a region of undamaged spinal cord is shown. This section is 40 μm thick, and the spinal cord was approximately 2.9 mm wide. In (A), an unadulterated histological image stained with hematoxylin and eosin was captured to the computer (refer to methods). In (B), this same image was first converted to a greyscale image and then convolved by the averaging of every pixel value to its adjacent pixel values. This results in an image, in which a more restricted (i.e. less extended) set of pixel values can be used to produce the final three-dimensional reconstruction that does not depend on the prior defining of physical boundaries as in the tiling procedure (Fig. 1A). In (C), the section shown in (A) and (B) is sandwiched between the two adjacent serial histological sections producing an amalgamation of three separate convolved sections. This procedure averages various aspects of the image, reducing or eliminating irrelevant or minor anatomical details such as small tears in one of the histological sections or extraneous spinal cord material projecting from the main image produced during histological sectioning (large arrow). C, central canal; G, grey matter; and W, white matter. Rostral is at the top of the images.The refinement of the isocontoured 3D image through filtering is shown in (D) and (E). In (D), is an isocontoured image of the spinal cord grey matter extracted from the data set shown in (A). Note that isocontour values numerically close to those comprising largely the grey matter embedded within the spinal cord segment data set have not been convolved and filtered from the reconstructed image. Convolution and the averaging of three adjacent convolved slices as described in the Methods for the entire data set allows the grey matter to be more clearly discerned in (E).

and a lack of extraneous isosurfaces that produce noise. For instance, the gradient integral (yellow waveform) indicates prominent surfaces in the data. Therefore, selecting isovalues at the peak(s) of the gradient integral displays structures of interest. Selecting the isovalue at the peak of the surface area signature (red waveform) reconstructs the noisy part of the data. Not only are features of interest imaged but also extraneous artifacts in the histological sections that contain the same pixel intensity resulting in large surface area measurements. Therefore, isovalues at the valleys of the surface area wavelength are often selected to better discriminate structures of interest. The isovalue selected in the spectrum at the top of Fig. 2 produced the 3D surface reconstruction of the ED1-labeled injury site shown at the bottom of Fig. 2.

The surface area and volume signatures are low degree spline curves, so exact quantification is provided in real time, by simply evaluating these linear B-spline functions. The B-spline function is an exact representation of the area value. We evaluated the spline polynomial instead of computing the intersection triangle and its area. Since the surface area of an entire isosurface is the sum of the areas inside each cell, we computed the overall area spectrum by summing together the B-splines of all the cells. To determine the volume contained inside each isosurface, we needed to compute the integral of the isosurfaces. Using a piecewise polynomial formula, we integrated each polynomial obtaining a new spline function representing the volume inside the isosurfaces.

2.7.3.1. Filtering process for the isocontouring method. In order to distinguish features of anatomical importance during isocontouring, a filter was applied to the data set of optical slices (Fig. 3). The histological sections of each spinal cord were convolved to reduce noise. Convolution normalized values of all pixels in a slice by replacing

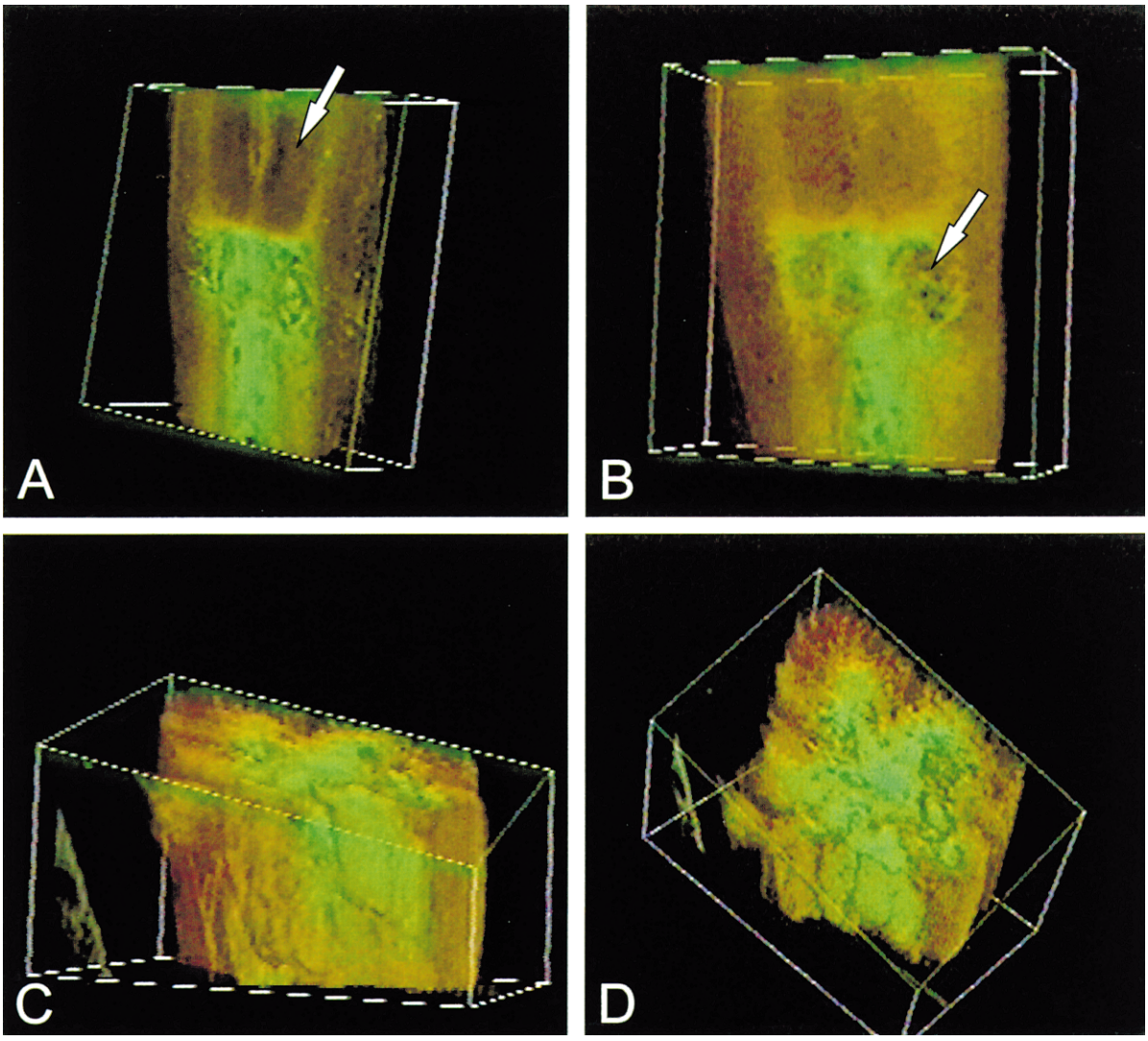

Fig. 4. Volumetric texture imaging of a segment of a spinal cord injury. All views presented here are rotations and/or sectioning of a three-dimensional visualization of a spinal cord segment containing a compression-produced lesion (refer to Fig. 1A and B). The bright green area is the lesion embedded within the semitransparent brown of the undamaged spinal cord tissue surrounding it. In (A), the image opacity was managed to show the twin horns of spinal cord grey matter (arrow) and in (B), to more clearly show cavitations within this zone of injury (arrow). This longitudinal/horizontal series of histological sections produced the longitudinal views of (A) and (B), which were additionally sliced by management of the image to produce the oblique transverse plane shown in (C), and the cross-sectional view shown in (D). Thus, the ability to view any "slice" or plane of the volume texture three-dimensional image is possible as is the ability to vary its opacity displaying features of interest that may be embedded within the image. However, quantitative querying of these types of images was not possible.

each pixel with a weighted average of the nearby pixels (Fig. 3B). To diminish artifacts and histological defects, the slices were averaged together. Averaging the optical slices combined overlapping groups of three slices into a single image resulting in the same number of averaged images as original slices (Fig. 3C). Averaging allowed only biological features that are consistent in two or more slices to be three-dimensionally reconstructed.

2.8. Statistical evaluation

Comparison of 3D visualization measurements provided here used a paired, two-tailed, nonparametric (Wilcoxon or Mann-Whitney) test for significance. Computations were performed using Instat© software.

3. Results

Each of the three approaches evaluated in this report was based upon different mathematics or algorithms and provided a different means to view the spinal cord and its experimental injury. We first summarize the three methods and their relative differences, and follow this summary with a detailed qualitative and quantitative comparison of the 3D

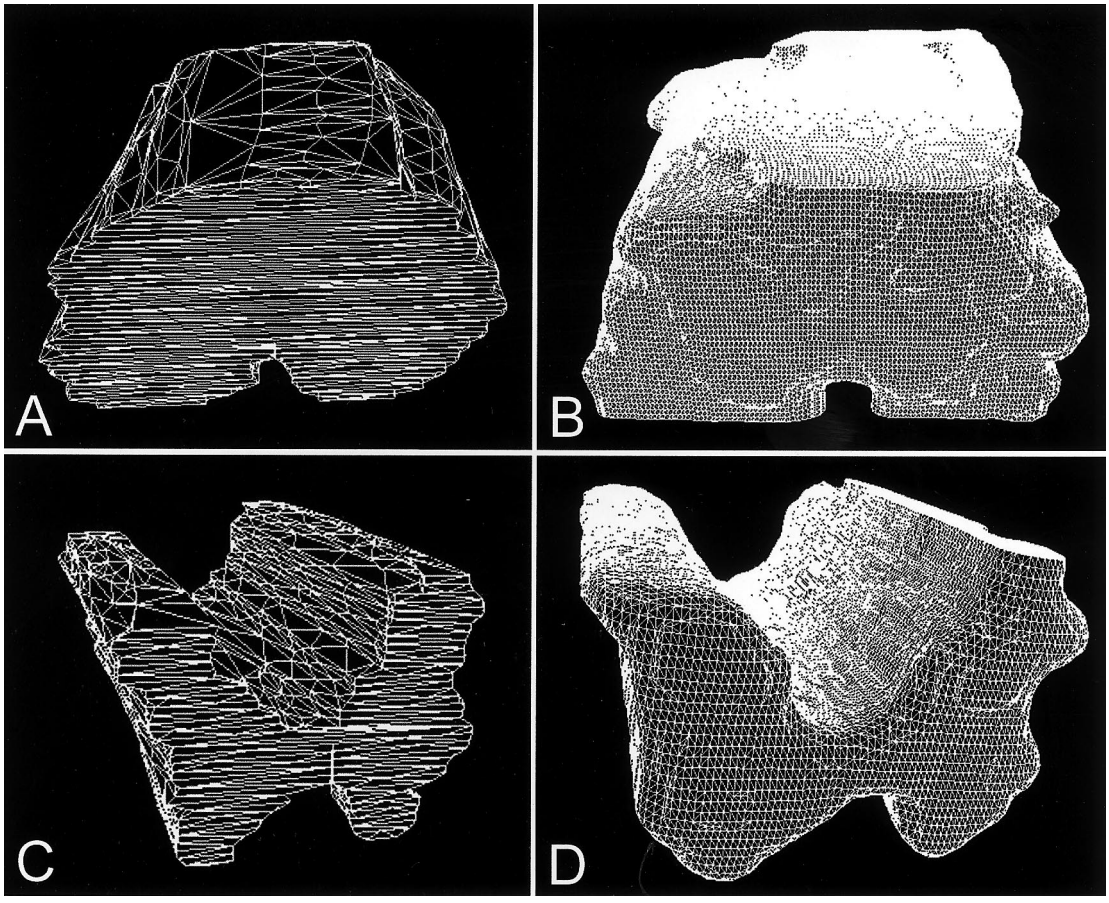

Fig. 5. Wireframe images derived with different surface reconstruction algorithms. All images shown were reconstructed from a segment of undamaged spinal cord (approximately 1/2 vertebral segment in length, 42 longitudinal/horizontal histological sections of 40 μm thickness comprised the data set). The 3D images in (A) and (B) show this entire data set (note the ventral fissure of the spinal cord segment at the bottom of the images in both (A) and (B)), while only the grey matter is shown following extraction from the data set in (C) and (D). In (C) and (D), note the characteristic "butterfly" shape of the grey matter due to the upward projecting dorsal horns and the ventral horns at the bottom of the images. In (A) and (C), the images were produced by surface tiling algorithms, while the reconstructions in (B) and (D) were generated by isocontouring algorithms. Both algorithms produced images based on polygonal primitives. The triangulations generated to form the 3D image are larger and more apparent in (A) and (C), but less conspicuous and providing more surface detail in (B) and (D). Note that both types of algorithms provide very similar three-dimensional images from an identical data set. Also note that pathological regions of spinal cord produce reconstructed images that are foreign or less familiar, while data sets such as this demonstrate that lifelike and familiar forms are generated by the same approaches. Quantitative evaluation of this data set is provided in Table 1.

images that were constructed by each of the three approaches.

3.1. Volumetric texture imaging

This approach was based on volume rendering algorithms that made use of the various differences in pixel values arising from the differences in the staining of cells (or groupings of similar cells) produced by the histological treatment of the tissues. Volume texture imaging provided a 3D image of the biological specimen in which much of its true character was preserved. This result was achieved because the 3D image was constructed from digitized serial sections without any computer-assisted manipulation of the specimen's features. The final volumetric image had a realistic, visual texture reminiscent of the actual spinal cord specimen. This final image could also be manipulated, for example made more transparent or more opaque. This allowed us to emphasize certain features such as pathological cavitations and cysts that in life would likely be filled with fluid (Fig. 4A and B). The final three-dimensional Volume Textured Image could also be rotated to provide any arbitrary view of the specimen or cleaved in any arbitrary plane to provide other structures of interest embedded within the image (Fig. 4C and D).

3.2. Surface tiling reconstruction

Surface Tiling algorithms required that the investigator scribe the boundaries of regions of interest within each 2D histological image captured to the computer. This generated sets of 2D contours. The space between the contours was then converted into a series of triangles (called primitives) in order to construct a 3D image by the amalgamation of all

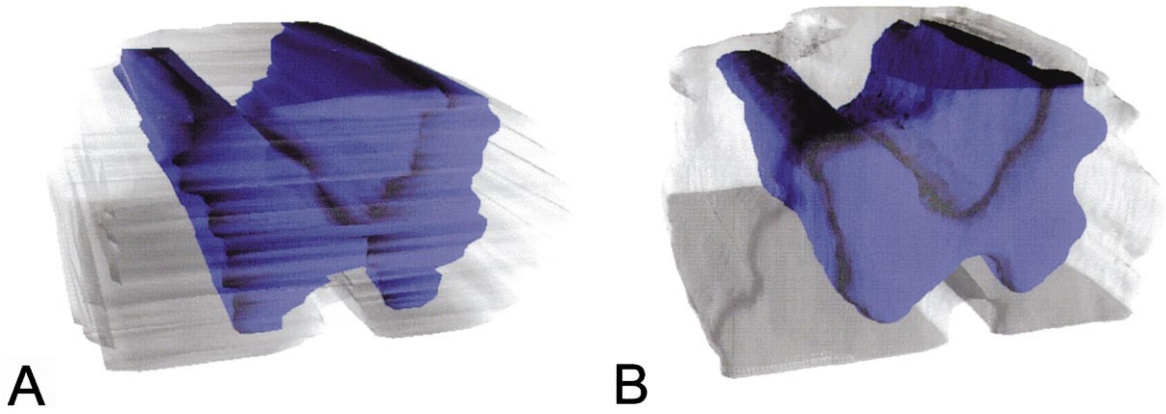

Fig. 6. Qualitative comparison of surface tiling and isocontouring approaches to building the three-dimensional image of an uninjured spinal cord. In (A), an uninjured spinal cord data set is shown by surface tiling reconstruction, in (B), the same data set by isocontouring (refer to Figs. 3 and 5). The white matter is made transparent so the central grey matter (blue) is revealed. The dorsal aspect is to the top of the page and the rostral end of the segment is shown facing the observer. The spinal cord segment is 3.2 mm long. The surface areas and volumes of select characteristic features are provided in Table 1.

of the contours derived from all histological sections comprising the data set. These surfaces were then revealed as a tiled mesh or "wireframe" (Fig. 5A and C), or as a smooth surface (Figs. 1B, C, and 6A). These images were not "lifelike" when compared to volume texture imaging. Rather, they were accurate models of the biological specimen that could be used to emphasize particular surfaces of structures or embedded structures that were a part of the final 3D image (Figs. 1, 6, and 7). Surface Tiled Images could also be interrogated to provide quantitative measurements of surface area and volume of any structure that was a component of the final 3D image. Finally, the algorithms used to construct surface tiled images allowed dynamic navigation, that is, placing the observer inside the 3D image to move about at an arbitrarily chosen rate of speed and direction and arbitrarily viewing chosen structures from any angle.

3.3. Isocontouring surface reconstruction

This was the most novel set of mathematics applied to 3D reconstruction of 2D spinal cord injury data sets. The algorithms underlying this method reconstructed 3D surfaces from pixels that had the same intensity or color value — a so-called "isovalue" (Fig. 2). Isocontours derived from shared specific sets of isovalues were converted to boundaries, i.e. bounded contours. Sets of boundaries were then derived within each 2D data set and were analogous to the boundaries produced by the manual methods employed during Surface Tiling, except that these boundaries were not manually traced by the investigator (Fig. 5B and D). The limits of the pixel values sampled to form isocontours was predetermined by the investigator, and the isosurfaces were then rendered by the computer without human interaction with the data set. This also reduced the time required to produce the 3D image, since manual tracing of contours on each captured 2D histological view was not needed. Isocontouring allowed quantitative querying of the surface area and volume of the various components of interest present within the final 3D reconstruction and dynamic navigation of the observer "into" the image (see below).

3.4. Registration of serial histological sections

The steps taken prior to 3D rendering were the most time-consuming aspects of the entire visualization process for all three methods. Unlike CT, MRI, and confocal microscopy, registration of histological sections is not automatic. Alignment and ordering of light microscopic sections within the data set must be done by the investigator. Registration involves correcting the translational positioning of each histological section on top of the next section, the degree of X–Y rotation of each section, and sometimes the warping or stretching of individual sections. We elected to register histological sections during capturing of the video image using a 'best-fit' method of matching each consecutive section with its neighbor. Fig. 1B and C shows the surface of the spinal cord lesion embedded within one of the histological sections used to three-dimensionally reconstruct it. The image illustrates proper registration of slices and its impact on the subsequent 3D surfaces.

3.5. Filtering of optical slices for isocontouring reconstruction

The surface tiling approach selected structures of interest differently than the volume texturing and isocontouring approaches. For both volume texturing and isocontouring methods, the ability to discriminate objects of biological importance from the data set of slices is dependent upon pixel value differences within the histological sections. Therefore, the tissue quality and contrast in staining of the histological sections were very important for high-definition 3D reconstructed images. Difficulties that arise during 3D reconstruction with pixel-based algorithms rested in the problems characteristic of

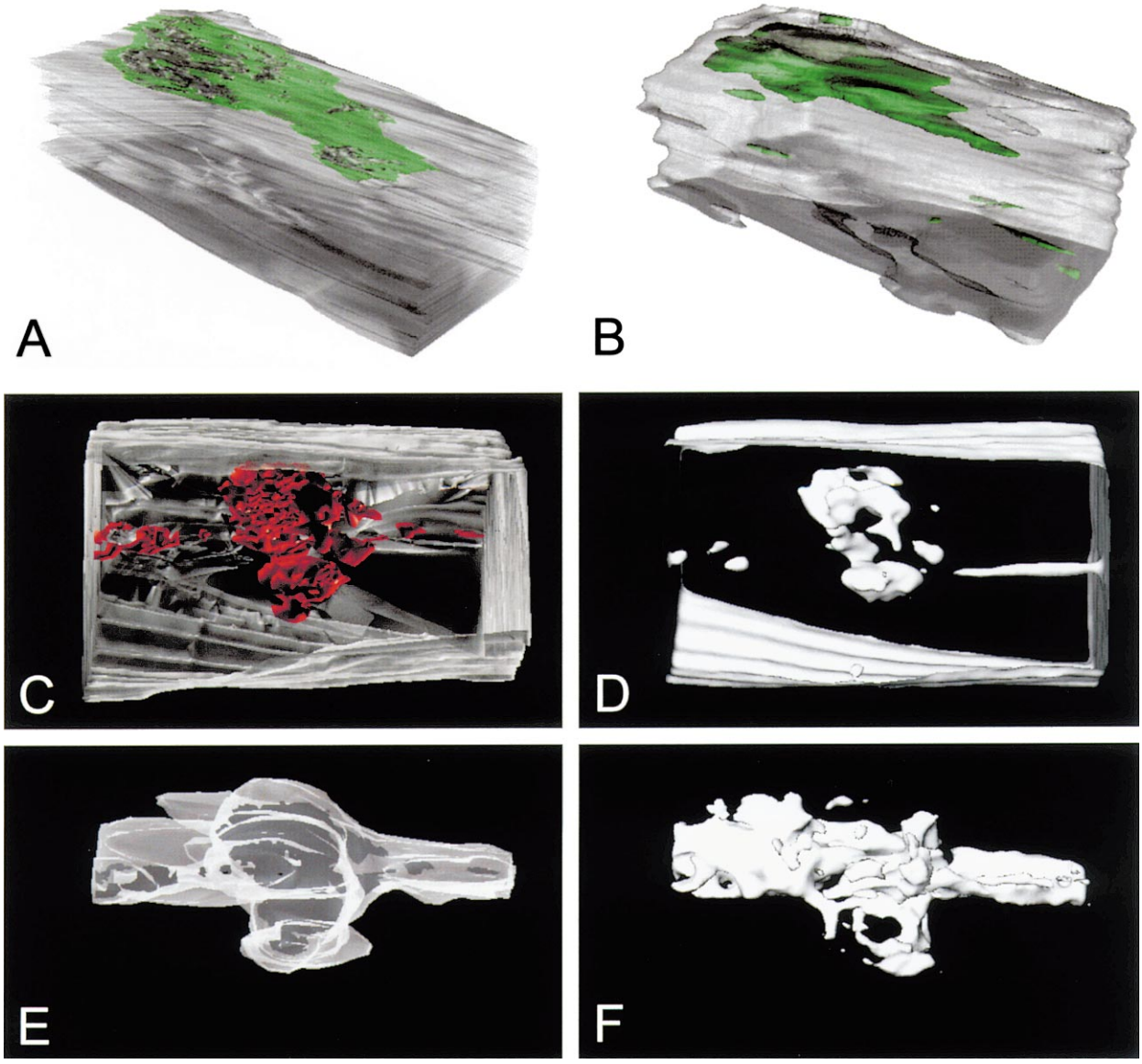

Fig. 7. Qualitative comparison of surface tiling and isocontouring approaches to building three-dimensional images of injured spinal cords. In (A), a three-week old spinal cord injury data set is shown by surface tiling reconstruction, in (B) by isocontouring algorithms (refer to Fig. 1C). The lesion shown in green is asymmetric and resides in the dorsal half of the spinal cord. Caudal is to the right. This spinal cord segment is 4.2 mm long. In (C) and (E), a second more severe, three-week old spinal cord injury data set is shown rendered by surface tiling reconstruction and in (D) and (F) by isocontouring algorithms (refer to Figs. 1B, 2, and 4). Rostral is to the left of the image and the ventral surface is facing the observer. In (C), the embedded cysts are shown in red pseudocolor. In (D) and (F), the cysts and lesion were not colored, but easily revealed for comparison against background. In (D), the central canal is disrupted by severe cavitation in the center of the segment. The rostral and caudal ends of the central canal can be seen projecting toward the cysts. The caudal end extends further in this spinal segment. The surface areas and volumes of select characteristic features are provided in Table 1.

histological sections including: (1) artifacts; (2) noise; and (3) histological defects.

1. Artifacts are extraneous materials captured along with the spinal cord segment. Artifacts appear under the coverslip but are not part of the tissue to be imaged, for example torn parts of dura mater or spinal roots (Fig. 3A, arrow).
2. Noise is extraneous pixels on an optical slice that have the same value as the pixels that composed the cells or structures to be visualized. For both volume texturing and isocontouring methods a single specified isovalue displayed not only the object of interest but also nonessential points with the same pixel value in other structures (Fig. 3D).
3. It is common to have defects like tears, shredding, or folds in histological preparations, which are exacerbated as histological section thickness is reduced for higher resolution light microscopy. These flaws rarely affected the overall morphology of structures within the entire

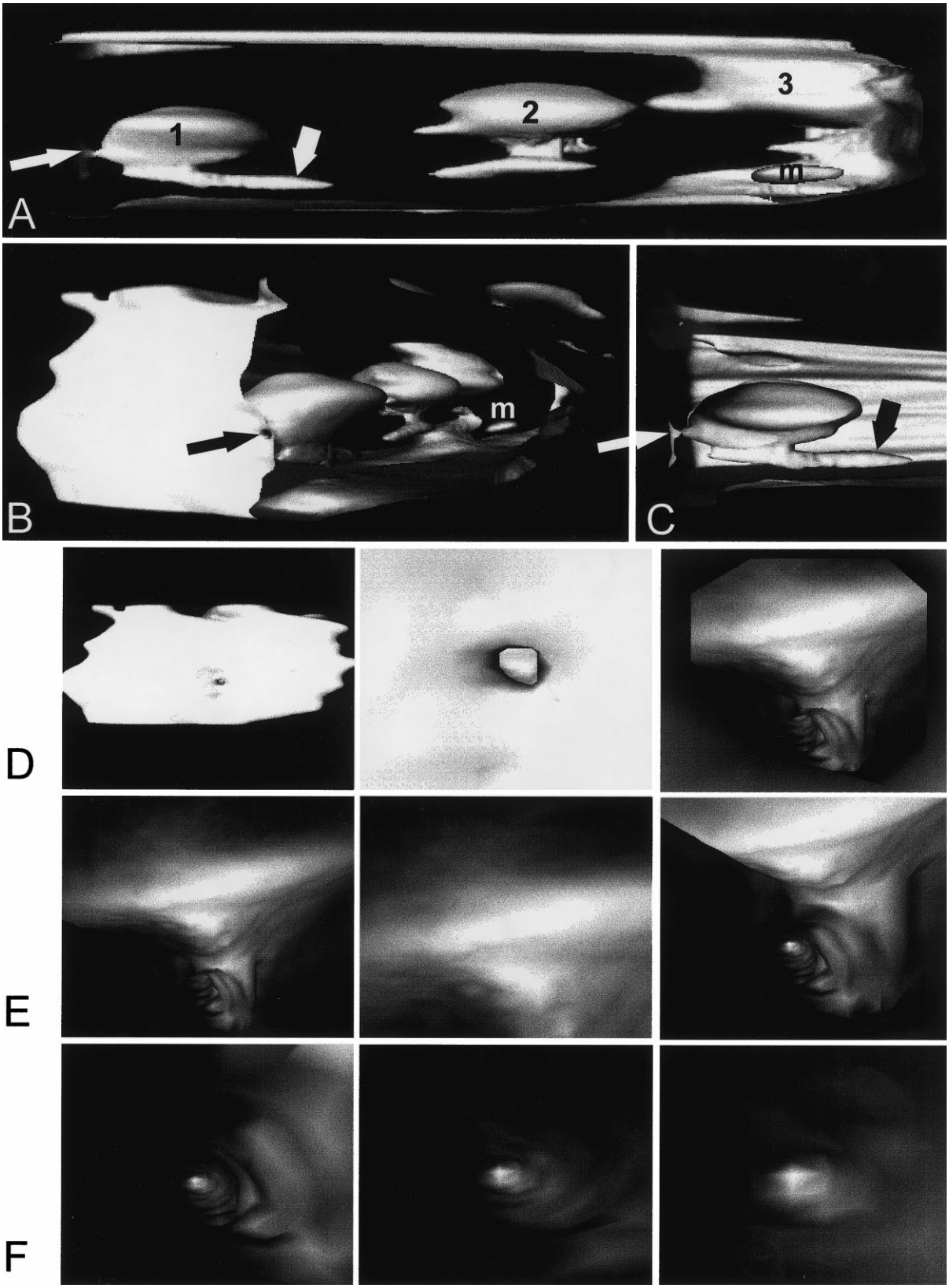
A
1
2
3
m
B
m
C
D
E
F

Table 1
Quantitative comparisons between surface tiling and isocontouring using normal and chronically injured spinal cord segments. The surface areas and volumes of select characteristic features of a spinal cord injury are measured from the 3D reconstructions of a normal and two injured spinal cord segments. Certain features could not be quantitatively compared because of algorithmic differences between surface tiling and isocontouring methods. Selection and 3D reconstruction of the injury site was different for each method. Surface tiled lesions comprised of the injury-recruited macrophages, cysts, and decomposing parenchyma. Afterwards the measurements of the largest cysts were subtracted from the lesion (refer to Fig. 7E). However, isocontoured lesions included only macrophage accumulations (Fig. 7F). Thus, only the combined surface area and volume measurements of the three spinal cord segments and grey matter of the uninjured spinal cord could be statistically compared ($(n = 8)$. (*) These values were calculated with another utility because the biological feature had to be separated from other concurrent isosurfaces (refer to Section 3). Note that isocontouring algorithms produced characteristically lower values for any queried region (see Section 4)

Spinal cords	Uninjured		First injured		Second injured	
3D Surface reconstruction methods	Surface tiling	Isocontouring	Surface tiling	Isocontouring	Surface tiling	Isocontouring
Cord surface area (mm^2)	38.5	28.0	45.4	34.3*	55.2	42.3
Cord volume (mm^3)	12.2	8.7	9.2	6.9	14.3	13.2
Grey matter surface area (mm^2)	27.8	17.1	N/A	N/A	N/A	N/A
Grey matter volume (mm^3)	4.2	2.9	N/A	N/A	N/A	N/A
Lesion surface area (mm^3)	N/A	N/A	20.7	10.5	12.9	8.4
Lesion volume (mm^3)	N/A	N/A	1.5	0.5	0.8	0.6
Cysts surface area (mm^2)	N/A	N/A	9.2	3.0*	N/A	N/A

data set, but they could be incorporated into the final 3D image. Differences in the intensity of staining between sections were not often observed but could be corrected by altering the brightness levels of the captured optical slice. In order to discern anatomical objects of interest during isocontouring, we applied a filter (see Methods) to each optical slice in our data sets to reduce the significance of superfluous information (Fig. 3D and E). However, during the contour tracing process used in surface tiling, these pixel value faults can be ignored.

3.6. Qualitative and quantitative comparison of 3D surface reconstructions

Only isocontouring and surface tiling permitted quantitative interrogation of the 3D reconstruction. Both algorithms developed triangulated wireframes as the framework for their 3D surfaces. The calculation of volume and surface area was accomplished from these closed, 3D tiled meshes (Fig. 5). Therefore, we were able to qualitatively and quantitatively compare the same 3D biological objects reconstructed by both visualization methods.

We chose to compare these two methods using a sample of three spinal cord segments, two of which had been injured. Fig. 6A and B shows a qualitative comparison between these methods for a normal, uninjured spinal cord. Both surface tiling and isocontouring algorithms produced 3D surfaces of this spinal cord that were morphological similar. The normal spinal cord was included in our evaluations as the shape and character of this anatomy was familiar. This is in contrast to 3D reconstructions of injuries that are highly variable in their anatomical character and their 3D morphologies are not well known.

Fig. 7 shows a qualitative comparison of chronically injured spinal cords. Both surface tiling and isocontouring methods produced similarly shaped 3D structures. These three-dimensionally reconstructed injuries were consistent with earlier gross pathological descriptions of rat spinal cord injuries obtained using conventional histological methods [7,23]. However, isocontouring did a better job of imaging tube-like structures such as the central canals shown in Figs. 7D and 8.

In Table 1 we quantitatively compared surface area and

Fig. 8. Dynamic navigation into a spinal cord injury reconstructed by isocontouring algorithms. This reconstructed data set shows a segment of rat spinal cord containing an injury produced by piercing its surface with a sharp probe during the transplantation of a piece of striated muscle taken from the same animal (refer to Methods). The reconstructed 3D image was managed to clearly show the outside perimeter of the spinal cord and particularly three large cysts (numbered 1–3) that formed within it in a longitudinal array. The injured spinal cord is presented with its dorsal (posterior) surface up and the rostral end to the left. The thin arrow points to the central canal of the spinal cord, easily viewed in (A), (B) (a rotated view of (A)), and (C). The wide arrow in (A) points to a longitudinally extended component of the most rostral cyst. This pathological fluid-filled "tube" is also marked with the black arrow in view (C). m, inserted piece of striated muscle graft.Rows D, E, and F demonstrate a navigation into the rostral opening of the central canal marked in (A), (B) and (C). The rows as read from left to right probe deeper into the canal opening into cyst number 1 (final view of row D). Row E shows internal features of the cyst after entering its rear opening, its roof (second view), and in the third view its opening into the small caudally extending tube (refer to wide arrow in (A) and (C)) in that order. In row F, the observer continues to probe deeper entering the small tube extending off the cyst caudally to its endpoint. This algorithmic approach allowed such navigation to be dynamic that is moving at a rate of speed and with panning ability controlled and directed by the user.

volume measurements from all our spinal cords to determine similarity in quantitation between surface tiling and isocontouring. Because of algorithmic differences between both these 3D reconstruction methods, we were unable to compare the measurements of every anatomical feature of the spinal cord that we three-dimensionally imaged. For instance, a quantitative comparison of injury sites between both methods was not possible. The surface tiled lesion in Fig. 7E included the labeled macrophages, pathological cysts, and the decomposed spinal cord parenchyma. Subsequently, the larger cysts were selected and their volumes were subtracted from the total lesion volume. In contrast, the isosurfaces of the injury site in Fig. 7F enveloped only the areas of the set of histological sections that shared a common pixel value, specifically the isovalue for ED1-labeled macrophages. Thus, isocontouring produced a more intricate lesion surface with a smaller surface area and volume than produced by the surface tiling method. There was a statistically significant difference between surface tiling and isocontouring methods for the combined volume and surface area measurements of the grey matter and spinal cord segments ($n = 8$, $P = 0.008$).

Occasionally, when an isovalue was chosen during isocontouring, two or more distinct structures were generated concurrently. In Fig. 7D both the entire spinal cord segment and the cysts within were rendered at the same time from the same isovalue. However, with an additional software utility we were able to separate multiple, biological structures from each other. We were then able to calculate surface area measurements for each of these separated structures (Table 1, asterisks). During this study volume quantitation of concomitant sets of isosurfaces was not possible.

We also applied other 3D quantitative approaches used to calculate volume and surface area of the spinal cord injury [12,13] for comparison to our 3D techniques. Past quantitative approaches have been based upon the principles of 2D morphometry and best-fit geometric equations. Two-dimensional morphometry was accomplished by multiplying the unit area of a region of interest by the section thickness for each serial histological section, the sum of which equaled the volume of the 3D structure. The best-fit principle compared the 3D structure of interest to a known geometric shape (i.e. an elliptical cylinder or a sphere). The surface area and volume formulas of the geometric shape were then calculated using the measurements of the histological tissue. Volume and surface area measurements computed by the isocontouring method were not significantly different from 2D morphometric and geometric best-fitting approaches ($n = 8$, $P > 0.4$, Wilcoxon). Quantitation by surface tiling was not significantly different from these approaches as well ($n = 8$, $P > 0.1$, Wilcoxon).

3.7. Three-dimensional dynamic navigation

The value of three-dimensional imaging was enhanced when a 3D model was animated. Motion added depth and texture to a 3D reconstructed spinal cord, not often evident when still images were viewed. When pathological cavities or cysts within the lesion were viewed following 3D volumetric texture imaging, certain rotations of the 3D image allowed the observer to look dorsal/ventrally through the cavitations of the spinal cord injury (Fig. 4).

Besides rotation and translation of the 3D object, panning and zooming were features that enhanced an understanding of the injury through visual inspection. Particularly with isocontouring and surface tiling methods, the user's vantagepoint of the 3D object did not have to be static. A structure could be viewed from any position, even from the inside peering outwards. This was useful when exploring internal structures such as the cystic cavities that occurred at the injury site (Fig. 8A–C). By combining zoom capability with object positioning, we were able to navigate through any structure within the 3D image. In rows D, E, and F of Fig. 8 the vantage point of the user moved through the opening of the central canal as it bifurcated dorsally into a spherical cyst and ventrally into a protruding tube-like structure that appeared to be continuous with the central canal and the first cyst. Dynamic navigation showed the "tube" not to be continuous with other nearby structures.

4. Discussion

Three-dimensional visualization grants a level of anatomical examination that is not possible by conventional histology. This is especially true in the study of spinal cord injury where multiple pathological features are embedded within each other. Only through training and experience does an investigator usually derive a mental construct of the 3D shape of the injury. Additionally, the 3D character of a spinal cord injury is still more elusive because of the variety of injury models used (i.e. compression, contusion, or transection injuries and acute or chronic injuries), species differences, and the different methods in which the lesion is examined (i.e. stains and planes of sectioning). Therefore, morphological comparisons between different types of spinal cord injuries are difficult to perform without 3D imaging.

Not only is the 3D character of the injury site observable, but the spatial relationship of structures to each other is also shown, especially when structures are embedded within one another or very complex. Using a transparency function, 3D reconstruction was useful at elucidating hidden structures and determining their proper spatial arrangement. In one example, the injury site within a segment of spinal cord, approximately one vertebral segment long, contained cysts or cavitations which in turn, contained an island or aggregation of macrophages floating freely within one of the largest cysts [14]. Also of significance was the relationship of the cysts to the central canal shown in the puncture spinal cord injury (Fig. 8).

New acquisition hardware and 3D reconstruction software

has made 3D imaging easier and quicker. We compared three different visualization algorithms to produce 3D computer images. There were benefits and disadvantages to each approach. A main advantage of the 3D surface reconstruction methods, surface tiling and isocontouring, was the ability to quantitatively interrogate the tiled surfaces that were produced. This ability greatly expanded the functionality of 3D reconstruction from biological imaging to morphometric analysis. To our knowledge, this is the first time measurement of the volume and surface area of injured spinal cords and the pathological structures embedded within was possible using the reconstructed 3D images themselves. This capability could be used to evaluate the success of an experimental treatment aimed at ameliorating necrosis.

4.1. Histological consideration

We used every section within a tissue for our 3D reconstructions in order to preserve visualization and quantitation accuracy. However, many have chosen to use multiples of sections [13,24–27], presumably to save capturing time and/or disk space from storage of slices and large 3D reconstructions. Additionally, large 3D reconstruction or volume visualization data sets take longer to render. If every third or every tenth section is used, a smoother 3D object may be produced at the expense of querying precise 3D measurements. Interpolating large gaps between consecutive sections during 3D reconstruction would invariably lead to inaccuracies in 3D visualization and subsequent quantitation. The necessity for precise representation of the 3D visualization must be weighed against the effort required to produce the 3D image.

We also used longitudinal histological sections instead of transverse sections, in part because more transverse sections are required to reconstruct a spinal cord segment of equal length. Moreover, at the chosen magnification the entire unit area of the lesion was contained within each longitudinal histological section.

4.2. Registration of serial sections

The registration of light microscopic histological sections during or after image capturing is critical. Image registration problems include; position and rotation of serial sections, shredding and folding of individual sections, shrinkage from fixation and dehydration, and compression and stretching introduced during sectioning [25,28].

Many registration methods require fiducial markers of some sort. Fiducial markers maybe inherent to the histological tissue; such as the boundaries of anatomical structures, blood vessels, or populations of identifiable cells [1,8,26,29,30]. Man-made fiducial points have also been used by: (1) introducing holes into the tissue [31,32]; (2) injecting ink or colored paraffin into holes in the embedding block external to the tissue [33]; (3) notching hatchmarks along the edges of the embedding block [2]; (4) inserting guideposts around the tissue prior to sectioning [24,31,34]; and (5) using externally embedded tissue collars [31,35].

Our method of registration aligned intrinsic fiducial markers within every section to the previous section in the data set. This ‘best-fit’ technique was effective for the histological sections we used and was similar to past techniques that aligned biological features inherent to the tissue sections [1,30,31,36,37]. Finding multiple intrinsic fiducial markers consistent in several consecutive sections, such as the boundaries of the tissue, central canal, cysts, and populations of identifiable cells, was not difficult with the tissues we three-dimensionally imaged. In our fields of view of injured spinal cords, we could capture an entire 4.2 mm long segment of spinal cord. Since we could use multiple fiducial markers and monitor the global shape of the tissue sections, best-fit registration was reliable.

Automated, computational techniques have been attempted to improve registration. These methods apply algorithms to: (1) superimpose the centroids and/or principal axes of sequential images [32,38,39]; (2) register the images from analyses of their auto- and cross-correlation functions [28]; (3) match consecutive contours using a best-fit method [40]; or (4) align successive sections using an exclusive-or index that is based upon image grey level distribution and tissue morphology [41]. Registration methods based upon the shape of the images, such as the center of mass and principal axes approaches, could cause misalignment when sections are naturally asymmetric [40]. Additionally, if generating contours from histological sections was necessary for registration, then another step would have to be added to the isocontouring and volumetric texture imaging approaches.

4.3. Volumetric texture imaging

Volumetric texture imaging is a commercially widespread method of 3D visualization. Since the final 3D image is produced by virtually stacking the optical sections, no additional 3D graphics are rendered (i.e. tessellation of wire meshes). Thus, the 3D image looks like the sum of its component optical slices. Biological features are then distinguished by the characteristic pixel intensities of the slices.

Animation of volume textured images increased conspicuity of embedded structures such as cysts. These 3D images maintained the original character of the tissue (Fig. 4), in contrast to 3D surface reconstructions (surface tiling and isocontouring) which are representations or models of the structures being imaged (Figs. 1B, 2, and 7C–F).

We could not quantitatively query volume visualizations or their subcomponents because during volumetric texturing, vague anatomical boundaries that are defined solely by voxel value make morphometry infeasible [40]. Unlike with surface tiling and isocontouring, the computer cannot distinguish the biological structures within the spinal cord injury

as separate entities without the generation of closed 3D surfaces. Theoretically, volume could be approximated by counting the voxels from a range of intensity values that compose a particular structure(s) of interest [32], but the noise of the sections does not permit structures to maintain a single density or voxel intensity. Additionally, we have not found a method of calculating surface area measurements from volume visualizations because wireframe surfaces are not generated to demarcate anatomical boundaries for the computer.

4.4. Surface tiling method

Stacking manually traced contours is a pervasive method for building 3D surfaces. Generally, this has been accomplished by scanning or digitizing camera lucida drawings, acetate overlays, or tracings from photographic prints [2,9,11,13,26–30]. Now image acquisition, registration, contour selection, 3D surface reconstruction, and finally structural quantification can all be accomplished via a keyboard and mouse.

Circumscribing contours by hand or a pointing device is the most tedious process in the surface reconstruction method. Thus, some are motivated to trace contours from every other or every tenth histological section [13,25–27]. Manually scribing contours around biological features can also introduce human subjectivity in the identification of pathological features. Clearly, no two humans can trace a complex histological structure within a data set of sections for 3D reconstruction identically.

Computer-automated extraction of contours from biological objects of interest has been attempted by others to reduce the labor and subjectivity of manual contour tracing. Popular methods of selecting areas of interest use segmentation or edge detection algorithms [39,40,42]. These algorithms attempt to select objects of interest based on their specific and uniform pixel intensity or by their distinct boundaries from the surrounding tissue. Since these physical qualities are hard to find consistently in each histological section, automated contour extraction is difficult.

4.5. Isocontouring method

In many regards, isocontouring is a combination of both volumetric texture imaging and surface tiling. Like volumetric texture imaging, isocontouring selects objects of interest based upon pixel intensity (isovalue) and then constructs a 3D wireframe surface similar to the surface tiling method. The isocontouring method was the newest visualization technique employed and by far, less labor intensive and time-consuming than surface tiling, since it does not require manual contour tracing. Isocontouring also eliminated the bias of contour selection.

Like surface tiling, isocontouring algorithms produced well-defined 3D surfaces which could be automatically quantified. Unlike surface tiling, the quality of the histological sections used for isocontouring must be very complete and as free of technical faults as possible since contour selection is based upon differences in pixel values. When contour tracing during the surface tiling method, one can ignore including flaws in the tissue, however that is not possible during isocontouring. Physical defects inherent to the tissue and a lack of contrast in tissue labeling make isocontouring more difficult.

4.6. Comparison between surface reconstruction methods

Qualitatively, all three spinal cord segments and subcomponents of the injury reconstructed by either surface tiling or isocontouring algorithms were very similar as evident in Figs. 6 and 7. Quantitatively, the measurements for the biological features we queried by the two different 3D surface reconstruction methods were significantly different. However, there was no significant difference between values derived from our 3D techniques compared to those from standard quantitative approaches. Thus, older 2D morphometric and geometric best-fitting approaches have shown that quantitation by surface tiling and isocontouring can be reliably achieved. We concluded that quantitative differences between surface tiling and isocontouring stemmed from differences in their algorithmic paradigms. While this seems paradoxical, the differences between surface tiling and isocontouring algorithms are likely the basis for the quantitative differences between the two, but not to reference methods.

Both surface tiling and isocontouring methods produced 3D wireframes, however as we have discussed they are based upon different reconstruction principles. The spinal cord measurements calculated by both methods were significantly different, in part because of different tessellation approaches. Typically soft tissues are smooth or rounded, so planar triangle primitives must conform to produce as natural a surface as possible. As illustrated in Fig. 5 the isocontouring method built 3D tiled meshes with smaller and more numerous triangles than did the surface tiling method. Therefore, isosurfaces were smoother than surface tiled 3D surfaces which could cause discrepancies in surface area and volume measurements. Slight differences in surface topologies generated by each technique possibly translated into quantitative differences, especially for surface area. Consequently, the isocontouring surface area measurements were consistently lower than those values derived by surface tiling reconstruction (Table 1).

Additionally, the filter used during isocontouring can also affect the overall size of the 3D isosurfaces since filtered slices are less resolved than the original histological sections. When using surface tiling methods, it is possible that manually tracing contours on each section could overestimate areas of interest to produce tiled surfaces that are more over-smoothed than those constructed using the isocontouring method. These algorithmic differences also probably contributed to the variance in measurements.

In a second report, we will examine in greater detail the

algorithmic and fundamental differences in quantitative querying between surface tiling and isocontouring and compare the accuracy of the quantitation methods by our 3D reconstruction techniques to standard 2D morphometric procedures using measurements from a larger sample of subjects. In addition, we have used these methods to compare the responses to treatment of spinal injuries with polyethylene glycol (Duerstock and Borgens, to appear elsewhere, see also Ref. [43]).

4.7. Navigation within biological structures

Dynamic navigation allows the observer to explore in more detail the relationship between anatomical features in the reconstructed 3D image. Instead of observing cell populations, nerve tracts, and cysts as separate entities, one can visualize them in a more lifelike way as connected parts of a system. In particular, we have provided visual evidence to the postulate that there may be a confluence of the central canal with the formulation of pathological cysts [27]. Thus, some cysts may be filled with cerebrospinal fluid.

Moreover, animation of a 3D object allows the eye to track features of interest based on motion, yielding powers of perception and discrimination unavailable to 2D plates of 3D visualizations. These features are particularly apparent during the rotation of the spinal cord images shown in Fig. 4 but are not as apparent when these images are still. This ability to pass on new and important features of a reconstructed image to others may only be allowed by electronic publishing, where the reader can animate these objects.

5. Summary

The pathology of mammalian spinal cord injury is usually defined as “central hemorrhagic necrosis”, where variable amounts of the peripheral white matter is spared while the central grey matter deteriorates. This condition had traditionally made microinvestigation of the injury site in experimental animal models of SCI only possible through histology. Unfortunately, histological examination is confined to two dimensions, unless the spinal cord is three-dimensionally reconstructed. Three-dimensional visualization grants a level of anatomical examination that is not possible by conventional histology. Not only is the 3D character of injured spinal cord segments shown, but the spatial relationship of structures to each other is also observable, especially when structures are embedded within one another or very complex. Additionally, instead of viewing from a single perspective, the ability to peer inside and manipulate the 3D reconstruction was extremely beneficial. 3D images could be observed from many different viewpoints. Rotation and zooming features were combined to allow observer navigation within the tissue. Animation of 3D objects provided depth perception, so spatial relationships of features could be better revealed.

We have evaluated three different algorithms to three-dimensionally visualize spinal cord injuries. These techniques are: (1) volumetric texture imaging; (2) surface tiling; and (3) isocontouring. There were certain advantages to each method. One such advantage when using the novel surface reconstruction methods, surface tiling and isocontouring, was the ability to automatically determine the volume and surface area of injured spinal cord segments and the structures embedded within them using the 3D reconstructions themselves. We were able to morphometrically compare these different reconstruction methods using three spinal cord data sets. We detected characteristic differences in the algorithms between these surface reconstruction methods that could influence quantitation. This was not observed when these methods were compared to morphometric data generated by older 2D morphometric and geometric best-fitting approaches found in the literature. In conclusion, we found 3D reconstruction to be a valuable tool for morphologically and morphometrically evaluating normal and pathological anatomical data.

Acknowledgements

We appreciate the technical aid of Debra Bohnert and Loren Moriarty during the conduct of these experiments and thank Carie Brackenbury and Jacqueline Libhart for aid in manuscript preparation. Financial support was provided by the Department of Defense — USAMRMC-DAMD17-94-J-4242 to R.B.B., AASERT — DAAH04-93-G-101 to R.B.B., CDC/CIC grant #R49/CCR509137 to R.B.B., AFSOR grants F49620-94-1-0080 to C.L.B., AASERT F69620-93-1-0553 to C.L.B., ONR grants N00014-96-1-0370 to C.L.B., AASDERT N00014-95-1-1025 to C.L.B., a grant of computer hardware from the Intel Corporation, and support of the Center for Paralysis Research and the Shastra Laboratory, Department of Computer Sciences, Purdue University by the Canadian Spinal Research Organization.

References

[1] Allen BA, Levinthal C. CARTOS II semi-automated nerve tracing: three-dimensional reconstruction from serial section micrographs. Comput Med Imaging Graph 1990;14(5):319–29.

[2] Hashimoto S, Kimura RS. Computer-aided three-dimensional reconstruction and morphometry of the outer hair cells of the Guinea pig cochlea. Acta Otolaryngol (Stockh) 1988;105:64–74.

[3] Salisbury JR. Three-dimensional reconstruction in microscopical morphology. Histol Histopathol 1994;9:773–80.

[4] DeVivo MJ, Whiteneck GC, Charles Jr. ED. The economic impact of spinal cord injury. In: Stover SL, DeLisa JA, Whiteneck GC, editors. Spinal cord injury: clinical outcomes from the model systems, Aspen Publications, 1994. p. 234–71.

[5] Bracken MB, Shepard MJ, Collins WF, Holford TR, Young W, Baskin DS, Eisenberg HM, Flamm E, Leo-Summers L, Maroon J. A randomized, controlled trial of methylprednisolone or naloxone

in the treatment of acute spinal-cord injury. N Engl J Med 1990; 322(20):1405–11.
[6] Borgens RB. Applied voltages in spinal cord reconstruction: history, strategies, and behavourial models. In: lllis LS, editor. Functional stimulation, vol. 3. Oxford: Oxford Medical Publications, 1992. p. 110–44 (chap. 5).
[7] Noble L, Wrathall J. Spinal cord contusion in the rat: morphometric analyses of alterations in the spinal cord. Exp Neurol 1985;88:135–49.
[8] Harris K, Stevens JK. Dendritic spines of rat cerebellar Purkinje cells: serial electron microscopy with reference to their biophysical characteristics. J Neurosci 1988;8(12):4455–69.
[9] Halliday GM, Cullen K, Cairns MJ. Quantitation and three-dimensional reconstruction of Ch4 nucleus in the human basal forebrain. Synapse 1993;15:1–16.
[10] Arndt S, Swayze V, Cizadlo T, O'Leary D, Cohen G, Yuh WTC, Ehrhardt JC, Andreasen NC. Evaluating and validating two methods for estimating brain structure volumes: tessellation and simple pixel counting. Neuroimage 1994;1:191–8.
[11] Navarro A, Tolivia J, Alvarez-Uría M. Hamster supraoptic nucleus: cytoarchitectural, morphometric, and three-dimensional reconstruction. Anat. Rec 1994;240:572–8.
[12] Blight AR. Delayed demyelination and macrophage invasion: a candidate for secondary cell damage in spinal cord injury. Cent Nerv Syst Trauma 1985;2:299–315.
[13] Bresnahan JC, Beattie MS, Stokes BT, Conway KM. Three-dimensional computer-assisted analysis of graded contusion lesions in the spinal cord of the rat. J Neurotrauma 1991;8:91–97.
[14] Moriarty LJ, Duerstock BS, Bajaj CL, Lin K, Borgens RB. Two- and three-dimensional computer graphic evaluation of the subacute spinal cord injury. J Neuro Sci 1998;155:121–37.
[15] Damoiseaux JGMC, Dopp EA, Calame W, Choa D, MacPherson GG, Dijkstra CD. Rat macrophage lysosomal membrane antigen recognized by monoclonal antibody ED1. Immunology 1994;83:140–7.
[16] Drebin RA, Carpenter L, Hanrahan P. Volume rendering. Computer Graphics (SIGGRAPH '88 Proceedings) 1988;22(4):65–74.
[17] Hall PM, Watt AH. Rapid volume rendering using a boundary-fill guided ray cast algorithm. In: Patrikalakis NM, editor. Scientific Visualization of Physical Phenomena (Proceedings of CG International '91), Berlin: Springer, 1991. p. 235–49.
[18] Cabral B, Cam N, Foran J. Accelerated volume rendering and tomographic reconstruction using texture mapping hardware. Symposium on volume visualization, ACM SIGGRAPH, 1994, p. 91–98.
[19] Bajaj CL, Coyle E, Lin K. Arbitrary topology shape reconstruction from planar cross sections. Graphical Models and Image Processing 1996;58(6):524–43.
[20] Bajaj CL, Coyle E, Lin K-N. Tetrahedral meshes from planar cross sections. Comp Meth Appl Mech Engng 1998 (in press).
[21] Bajaj C, Coyle E, Lin K. Boundary and 3D triangular meshes from planar cross sections. Proceedings of the 5th International Imaging Roundtable, Sandia National Labs, Report SAND 96-2301, VC-405, 1996. p 169–78.
[22] Bajaj CL, Pascucci V, Schikore DR. The contour spectrum. In: Yagel R, Hagen H, editors. Proceedings of the IEEE Visualization '97 Conference, New York: ACM Press, 1997. p. 167–75.
[23] Balentine JD. Pathology of experimental spinal cord trauma: I. The necrotic lesion as a function of vascular injury. Lab Invest 1978;39(3):236–53.
[24] Chawla SD, Glass L, Proctor JW. Three-dimensional reconstruction of disseminated cancer modules. Cancer Biochem Biophys 1981;5:153–61.
[25] Ross MD, Montgomery K, Cheng R, Doshay DG, Linton SW, Parnas BR. High performance computing applications in neurobiological research. Society for computer simulation, San Diego, CA, 1994, p. 120–5.
[26] Liss AG. Computer-assisted method for simultaneous three-dimensional reconstruction of highly magnified nerve endings and low-magnification contours of the spinal cord. J Microsc 1995;178 Pt: 2:160–4.
[27] Beattie MS, Bresnahan JC, Komon J, Tovar CA, Van Meter M, Anderson DK, Faden AI, Hsu CY, Noble LJ, Salzman S, Young W. Endogenous repair after spinal cord contusion injuries in the rat. Exp Neurol 1997;148:453–63.
[28] Hibbard LS, Grothe Jr RA, Arnicar-Sulze TL, Dovey-Hartman BJ, Page RB. Computed three-dimensional reconstruction of median-eminence capillary modules: image alignment and correlation. J Microsc 1993;171:39–56.
[29] Young SJ, Royer SM, Groves PM, Kinnamon JC. Three-dimensional reconstructions from serial micrographs using the IBM PC. J Electron Microsc Tech 1987;6:207–17.
[30] Martone ME, Zhang Y, Simpliciano VM, Carragher BO, Ellisman MH. Three-dimensional visualization of the smooth endoplasmic reticulum in Purkinje cell dendrites. J Neurosci 1993;13(11):4636–46.
[31] Gaunt WA, Gaunt PN. Three dimensional reconstruction in biology. Baltimore: University Park Press, 1978.
[32] Bron C, Gremillet P, Launay D, Jourlin M, Gautschi HP, Bachi T, Schupbach J. Three-dimensional electron microscopy of entire cells. J Microsc 1990;157:115–26.
[33] Vuillemin M, Pexeider T, Wong YM, Thompson RP. A two-step alignment method for 3D computer-aided reconstruction based on fiducial markers and applied to mouse embryonic hearts. Eur J Morphol 1992;30(3):181–93.
[34] Prothero JS, Prothero JW. Three-dimensional reconstruction from serial sections. IV. The reassembly problem. Comput Biomed Res 1986;19:361–73.
[35] Williams BS, Doyle MD. An internet atlas of mouse development. Comput Med Imaging Graph 1996;20(6):433–47.
[36] Deverell MH, Salisbury JR, Cookson MJ, Holman JG, Dykes E, Whimster WF. Three-dimensional reconstruction: methods of improving image registration and interpretation. Anal Cell Pathol 1993;5:253–63.
[37] Roesch S, Mailly P, Deniau JM, Maurin Y. Computer assisted three-dimensional reconstruction of brain regions from serial section digitized images. Application to the organization of striato-nigral relationships in the rat. J Neurosci Methods 1996;69:197–204.
[38] Bergognoni M, Crovetto A, Casali AM, Dellepiane S. Fast image processing for registration and 3D reconstruction of microscopical slice images. Proceedings of the Thirteenth International Conference of the IEEE Engineering in Medicine and Biology Society, Orlando, FL, USA, 1999, p. 1119–1120.
[39] Montgomery K, Ross MD. A method for semiautomated serial section reconstruction and visualization of neural tissue from TEM images. SPIE 1993;1905(1):114–20 (biomedical image processing and biomedical visualization conference).
[40] Toga A. Three-dimensional reconstruction. In: Toga AW, editor. Three-dimensional neuroimaging, New York: Raven Press, 1990. p. 189–210.
[41] Honghui G, Qunsheng P. An efficient alignment algorithm for 3D reconstruction of pulmonary alveolus from serial microsections. SPIE 1996;2644:2–68.
[42] Durikovic R, Kaneda K, Yamashita H. Imaging and modelling from serial microscopic sections for the study of anatomy. Med Biol Engng Comput 1998;36:276–84.
[43] Borgens RB, Shi R. Immediate recovery from spinal cord injury through molecular repair of nerve membranes with polyethylene glycol. J FASEB 2000;14:27–35.

Bradley S. Duerstock received a Bachelor's degree in Biomedical Engineering from Purdue University and in 1999 earned a PhD in Neurobiology. Currently, he is a Postdoctoral Research Associate at the Center for Paralysis Research, Institute for Applied Neurology in the School of Veterinary Medicine. His research interests include using 3D visualization to evaluate and quantify the anatomical and cellular changes that occur in the injured mammalian spinal cord over time and to examine the efficacy of experimental treatments to promote neurological recovery.

Chandrajit Bajaj is the CAM Chair in Visualization Professor of Computer Sciences at the University of Texas at Austin, as well as the Director of the Center of Computational Visualization. He graduated from the Indian Institute of Technology, Delhi with a Bachelor's Degree in Electrical Engineering, and received his MS and PhD degrees in Computer Sciences from Cornell University, Ithaca, New York. Prior to the University of Texas, Dr Bajaj was a Professor of Computer Sciences at Purdue University and Director of their Center for Image Analysis and Visualization. Dr Bajaj's research is in the areas of computer graphics, geometric modeling and data visualization. In particular, he develops novel approaches to representing, reasoning about, displaying and interacting with computer models of physical domains with associated physics. Current approaches include the use of combinatorial, and algebraic geometry to devise data structures that support multi-resolution approximations of very large domains and multiple function fields; an integrated parallel framework for domain modeling, physics calculations and interrogative visualization mapped onto high performance computational testbeds. Dr Bajaj has over 170 publications, has written two books and edited two other books in his area of expertise. He is Editor for the International Journal of Computational Geometry and Applications, as well as the ACM (association for computing machinery) journal Transactions on Graphics. He is on numerous national and international committees and foundations.

Valerio Pascucci obtained a "Laurea" degree in Electrical Engineering in 1993 at the University of Rome "La Sapienza", Italy. He moved to West Lafayette, Indiana, in 1995 as a visiting scholar at Purdue University, where he was admitted in the graduate school in 1996. In 1998, he moved to Austin, Texas, with a position of Senior Research Associate. In May 2000, he earned a PhD degree in Computer Science at Purdue University. For his thesis work, he also received an award from the UPE Honor Society for outstanding student research. He is a member of the ACM, IEEE, AMS and UPE Honor Society and has served as a reviewer for several journals (ACM Transactions on Graphics, Computer Aided Design, IEEE Transactions on Visualization and Computer Graphics, Journal on Algorithms) and conferences (IEEE Conference on Visualization 1999 and 2000, Vis'99 Late Breaking Hot Topics, Eurographics 1999, Solid Modeling 1999, WSCG 1998 and 1999). He currently has a research position as Computer Scientist in the CASC Department of the Lawrence Livermore National Laboratory.

Daniel R. Schikore is a Senior Developer at Computational Engineering International (CEI). He received his PhD from Purdue University in 1997. His research interests include feature extraction, surface extraction, multi-resolution data structures and algorithms, and rendering. He is a member of IEEE and ACM.

Kwun-Nan Lin received his BS from Chiao-Tung University, Taiwan, in 1982, a MS from University of Cincinnati in 1988, and a PhD from Purdue University in 1997. He joined Silicon Graphics, Inc. in 1997 and is currently working at Foundry Networks.

Richard Ben Borgens obtained a PhD in Biophysics in 1976 at Purdue University. He was the first National Paraplegia Foundation fellow at Yale University until 1980. He has been on the faculty of Purdue University since 1982, rising to the rank of Full Professor in 1990. He is currently the Director of the Institute for Applied Neurology, Center for Paralysis Research in the School of Veterinary Medicine in the Department of Basic Medical Science. He holds a second appointment as Professor of Biomedical Engineering in the School of Engineering. He has won numerous awards including: Iwao Yasuda Annual Award, Excellence in Biomedical Engineering Research, Society for Physical Regulation in Biology and Medicine (1998); Annual Pfizer Corporation Animal Health Award (1997); Distinguished Alumnus Award, University of North Texas (1994); Sagamore Award from the Governor of Indiana (1989) (past recipients include Harry Truman, Hoagy Carmichel, and Virgil Ivan "Gus" Grissom), Smith Kline Beecham Laboratories Annual Award, Research Excellence, Purdue University (1987), and the American Spinal Cord Society Annual Research Medal (1986). He has served on numerous executive boards and review panels for both private foundations and the federal government. His Center's research and the development of treatments for spinal injury have received national and international attention in both the printed media (Discover Magazine, The New Scientist, Time Magazine) and broadcast media (NBC Dateline, NBC Today Show, PBS, NPR).